1982AJ.....87..577W

THE ASTRONOMICAL JOURNAL VOLUME 87, NUMBER 3 MARCH 1982

THE ORIGIN OF THE KIRKWOOD GAPS: A MAPPING FOR ASTEROIDAL MOTION NEAR THE 3/1 COMMENSURABILITY

JACK WISDOM
California Institute of Technology, Pasadena, California 91109
Received 29 June 1981; revised 30 November 1981

ABSTRACT

A mapping of the phase space onto itself with the same low-order resonance structure as the 3/1 commensurability in the planar-elliptic restricted three-body problem is derived. This mapping is approximately 1000 times faster than the usual method of numerically integrating the averaged equations of motion (as used by Schubart, Froeschlé, and Scholl in their studies of the asteroid belt). This mapping exhibits some surprising behavior that might provide a key to the origin of the Kirkwood gaps. A test asteroid placed in the gap may evolve for a million years with low eccentricity (<0.05) and then suddenly jump to large eccentricity (>0.3), becoming a Mars crosser. It is possible that the asteroid could then be removed by a close encounter with Mars. As a first test of this hypothesis a distribution of 300 test asteroids in the neighborhood of the 3/1 commensurability was evolved for two million years. When the Mars crossers are removed, the distribution of initial conditions displays a gap at the location of the 3/1 Kirkwood gap. While this is the first demonstration of the formation of a gap, the gap is too narrow. The planar-elliptic mapping is then extended to include the inclinations and the secular perturbations of Jupiter's orbit. The two-million-year evolution of the 300 test asteroids is repeated using the full mapping. The resulting gap is somewhat larger yet still too small. Finally the possibility that over longer times more asteroids will become Mars crossers is tested by studying the evolution of one test asteroid near the border of the gap for a much longer time. A jump in its eccentricity occurs after 18 million years, indicating that indeed it may simply be a matter of time for the full width of the gap to open.

I. INTRODUCTION

Over 100 years have passed since the discovery of the Kirkwood gaps in the distribution of semimajor axes of the asteroids, yet there is still no adequate theory of their origin. Greenberg and Scholl (1979) give a review of the competing hypotheses and some of their difficulties. Briefly, there are four classes: (1) the gaps are only a statistical phenomenon, (2) the gaps are formed by purely gravitational forces, (3) the gaps form because asteroids near resonances tend to have larger eccentricities and hence larger probability of being removed by a collision with another asteroid away from the gaps, and (4) no asteroids were ever in the gaps.

The statistical hypothesis is that asteroids near commensurabilities undergo large variations in their semimajor axes, spending most of their time away from the commensurabilities, just as a pendulum spends most of its time away from the bottom of its swing. The time-averaged distribution could then display a gap. Schweizer (1969) calculated the orbits of numbered asteroids near the gaps and found that most asteroids did not cross the gaps. Wiesel (1976) studied the statistical hypothesis theoretically within the averaged planar-circular restricted three-body problem. He obtained depressions in the distribution but nothing resembling the observed distribution. According to Wiesel the most serious limitation in his theory is the truncation of the disturbing function to the terms of lowest order in eccentricity. I believe that a more serious limitation is the neglect of Jupiter's eccentricity, which introduces qualitative changes in the types of motion possible (see Froeschlé and Scholl 1977), especially the possibility of "ergodic" trajectories (Giffen 1973; Froeschlé and Scholl 1978). Although it is not the main thrust of this paper, I will show below that the statistical hypothesis fails under much more general assumptions than considered previously. I include the eccentricity of Jupiter, the inclinations, as well as the secular perturbations of Jupiter's orbit.

The gravitational hypothesis is that under the influence of gravitational forces alone, the semimajor axes of asteroids drift away from commensurabilities. The gravitational hypothesis has been studied analytically by Schubart (1964) in the averaged planar-circular restricted three-body problem. In this approximation the problem is completely integrable, and asteroids do not leave the gaps. Schubart's assumptions are clearly too restrictive, yet to lift any of the assumptions is to make the theory analytically intractable. The long-time evolution of dynamical systems is in general a very difficult and unsolved problem. The Kolmogorov-Arnol'd-Moser (KAM) theorem (see, e.g., Moser 1973) in certain special cases proves the existence of quasiperiodic trajectories. Though a tremendous advance in our exact understanding of dynamical systems, the KAM theorem is not a practical theorem in the sense that it applies only for sufficiently small perturbations where "sufficiently" is not precisely defined. The numerical experi-

 0004-6256/82/030577-17$00.90 © 1982 Am. Astron. Soc.

© American Astronomical Society • Provided by the NASA Astrophysics Data System

1982AJ.....87..577W

ments of Hénon and Heiles (1964) (and many others now) revealed a division of the phase space of simple Hamiltonian systems into quasiperiodic and "ergodic" regions for a range of perturbation strengths. The resonance overlap criterion (see Chirikov 1979, for a general review, and Wisdom 1980, for an application to the restricted three-body problem) provides some insight as to which regions of phase space will be "ergodic," but for detailed results there is no other recourse than numerical studies. Asteroidal motion at commensurabilities has been studied numerically by Scholl and Froeschlé (1974, 1975), who integrated the averaged equations of motion for the planar-elliptic problem as described by Schubart (1964, 1968). None of their fictitious asteroids were found to leave the gaps, though some did alternate between circulation and libration. One possible objection to this work is that the integrations were continued for only 100 000 yr, which is very short compared to the age of the solar system. Is it possible that over much longer times asteroids do drift out of the gaps? Arnol'd has discovered that dynamical systems may exhibit a very slow diffusion through phase space (see Chirikov 1979). However, Arnol'd diffusion does not occur in autonomous systems with only two degrees of freedom and since the averaged planar-elliptic problem has only two degrees of freedom, it has no slow diffusion. If more degrees of freedom are added, the possibility of diffusion must be considered. In particular, diffusion is possible in the unaveraged problem, i.e., the problem with high-frequency terms, and in the three-dimensional elliptic problem.

The validity of the collisional hypothesis was the primary topic addressed in the papers of Scholl and Froeschlé (1974, 1975). Using the averaging procedure for the planar-elliptic problem, they studied a large number of fictitious asteroids with initial conditions near the gaps. Their integrations generally covered a time interval of less than or near 50 000 yr, though a few were continued for 100 000 yr. The important question is whether or not the orbits show large eccentricity variations. Scholl and Froeschlé found that test asteroids close to the 3/1, 5/2, and 2/1 commensurabilities with either small initial eccentricity or moderate eccentricity near the borders of the observed gaps did not develop large eccentricities. No test asteroids at the 7/3 resonance developed large eccentricity. Since the Kirkwood gaps are clear of asteroids of all eccentricities, these results seem to militate against the collision hypothesis. The collision hypothesis is also doubtful because the collision probability depends weakly on the eccentricity, whereas the gaps have relatively sharp boundaries. Furthermore, an asteroid with low eccentricity near the 2/1 commensurability has a higher probability of collision than a high-eccentricity asteroid because of the sharp drop in the number of asteroids beyond 3.2 AU (Ip 1979).

Largely because of the failure of these studies to explain the Kirkwood gaps the possibility that asteroids were never in the gaps has started to be explored (e.g., Heppenheimer 1978). Since the dynamical hypotheses have not yet been fully disproved, it seems premature to abandon them for the more speculative theories of origin. I will not discuss these further.

In this paper I introduce a significant new method for studying asteroidal dynamics near commensurabilities, namely, I derive algebraic mappings of the phase space onto itself that have the same low-order resonant structure as the 3/1 commensurability. These mappings are derived by first analytically averaging the Hamiltonian to remove the nonresonant high-frequency contributions, the terms which are removed numerically by Schubart's averaging procedure. To this averaged, resonant Hamiltonian, I then add new high-frequency terms which are chosen so that the Hamiltonian becomes a series of periodic (in time) delta functions, each of which can be analytically integrated. Thus the averaged equations of motion for the mappings are identical to the averaged equations of motion used by Schubart, Giffen, and Froeschlé and Scholl (except that the mappings retain only the lowest-order terms in the disturbing function). Mappings have two principal computational advantages over Schubart's method of numerically integrating the averaged equations of motion: (1) mappings are about 1000 times faster, the integrations that lasted 40 min for Froeschlé and Scholl are reproduced in only a couple of seconds by a mapping; and (2) they are more accurate since they are purely algebraic and thus have the full accuracy of the computer. An important theoretical advantage is that the mappings have high-frequency contributions which are not present in the averaged equations of motion. The presence of high-frequency perturbations introduces some qualitative changes in the dynamics such as the "stochastic" separatrix and the possibility of the Arnol'd diffusion (see Chirikov 1979). I choose to study the 3/1 Kirkwood gap because it is the largest of the gaps, except for the 2/1 gap, and is not confused with the boundaries of the asteroid belt as is the 2/1 gap. There are no fundamental difficulties in deriving mappings for the other commensurabilities.

In Sec. II, I review the motivations for using the averaging principle. In Sec. III, I derive a Hamiltonian that approximates motion near the 3/1 commensurability. In Sec. IV, I derive the mapping for the planar-elliptic problem. I present in Sec. V some surprising results, and then study a distribution of 300 test asteroids for two million years. I extend the mapping in Sec. VI to include the secular perturbations of Jupiter's orbit and the inclinations. In Sec. VII, I reexamine with the full mapping the evolution of the distribution of 300 test asteroids for two million years. My conclusions are stated in Sec. VIII.

II. THE AVERAGING PRINCIPLE

All of the theoretical and numerical studies mentioned in Sec. I, except for that of Schweizer, who inte-

© American Astronomical Society • Provided by the NASA Astrophysics Data System

1982AJ.....87..577W

grates for at most only 2000 yr, rely on the averaging principle. The averaging principle has always played an important role in the study of the long-term evolution of the planets and asteroids. The averaging principle was introduced by Lagrange and Laplace (see Moulton 1970 for a historical summary) to argue that the secular terms which had appeared in earlier perturbation schemes were in fact the first terms in the expansions of purely periodic functions. The averaging principle was explicitly stated by Gauss, who calculated the long-period variations in the elliptic elements by replacing each planet by a ring of mass whose density was inversely proportional to the planet's velocity. Newcomb, Lindstedt, Poincaré, and many others (see Poincaré 1892 for a thorough discussion) extended this idea and demonstrated that it was possible to construct formal power series of purely periodic terms which satisfy the equations of motion of celestial mechanics. At each order in the construction of these formal series the averaged part of the perturbation is used to modify the unperturbed frequencies and the periodic part is removed by a canonical transformation. The existence of these formal perturbation theories seems to justify, then, the intuitive idea of the averaging method, i.e., that the basic dynamics is determined by the averaged equations of motion while periodic perturbations, which may be formally eliminated by an infinite sequence of canonical transformations, lead to purely periodic variations of the elements about this underlying evolution. Unfortunately, the canonical transformations which remove at each order the periodic part of the perturbation introduce in the next order the infamous divisors, which may become arbitrarily small. Thses small divisors are at the heart of Poincaré's famous theorem on the nonexistence of uniform integrals other than the classical ones and his subsequent proof that these formal periodic series generally do not converge. After proving this, Poincaré goes on to say that these series are still useful since they can be extremely good approximations for a long time. The difficulties of the small divisors were partially overcome in the work of Kolmogorov, Arnol'd, and Moser (see Moser 1973) who constructed a perturbation scheme which converges for sufficiently small and smooth perturbations, and frequencies which satisfy a diophantine condition (i.e., which are sufficiently irrational). The trick of the "superconvergent" perturbation scheme of Arnol'd is that the frequencies of the solution are held fixed, thus forever satisfying the diophantine condition and overcoming the small divisors, while the initial conditions are allowed to vary. This perturbation scheme again relies on repeated averaging. The KAM theorem proves by construction the existence of certain quasiperiodic motions. It says nothing about the regions of phase space that are excluded by its assumptions. In fact, numerical experiments (e.g., Hénon and Heiles 1964) seem to indicate that quasiperiodic motion is far more prevalent than is actually proved by the KAM theorem. One can argue then that it is only a matter of time before a more widely applicable convergent perturbation scheme is constructed.

On the other hand, it is known that trajectories which are not quasiperiodic can occur. It has been proved by Arnol'd (see Arnol'd and Avez 1968) for a particular Hamiltonian system that an unstable trajectory (nonquasiperiodic) can always be found for arbitrarily small values of the perturbation parameter. It is expected that this instability is a generic feature of nonintegrable Hamiltonian systems, and that it leads to the so-called "Arnol'd diffusion." The mechanism of the Arnol'd diffusion may be understood intuitively in the following way. First, there are resonances arbitrarily close to every point in plase space, because the frequencies, however irrational, can be approximated arbitrarily well by rationals. Each of these resonances possesses a separating trajectory, a separatrix, which divides the phase space into regions where the resonant combination of angles oscillates and those regions where it circulates. In a nonintegrable system these separatrices are broadened into very narrow stochastic layers (see Chirikov 1979). The width of these stochastic layers depends exponentially on the ratio of the nearest perturbation frequency and the basic frequency of oscillation of the resonant combination of angles. The width of these layers may thus be extremely small. This everywhere-dense network of stochastic layers has been termed the "Arnol'd web." Numerical experiments have indicated that motion in the exponentially small stochastic layers is well modeled as a diffusive process. That is why this unstable motion is called the "Arnol'd diffusion." In systems with two degrees of freedom, quasiperiodic trajectories confine the stochastic layers and Arnol'd diffusion is not possible. In cases where the motion is quasiperiodic, the averaged equations of motion may be expected to give a good approximation, the periodic perturbations being removed by an as yet unknown convergent-perturbation theory. But in cases where the averaging reduces the number of degrees of freedom to 2 or fewer, the averaging principle must fail for those initial conditions within the Arnol'd web, because diffusion is possible in the unaveraged system but is not possible in the averaged system. Thus Arnol'd (1978) says of the averaging principle: "We note that this principle is neither a theorem, an axiom, nor a definition, but a physical proposition, i.e., a vaguely formulated and strictly speaking untrue assertion. Such assertions are often fruitful sources of mathematical theorems."

Despite the fact that the averaging principle remains an intuitive assertion which is, strictly speaking, untrue, it has been used in essentially all theoretical studies of the long-term behavior of objects in the solar system. It is perhaps surprising at first, but the averaging principle has also been used in almost all numerical studies that span more than a few thousand years. The reason is simple. It is just too expensive to extensively study the unaveraged equations of motion. The averaging principle provides a compromise. Averaging the equations of mo-

© American Astronomical Society • Provided by the NASA Astrophysics Data System

1982AJ.....87..577W

tion eliminates the short-period variations, making the equations much less expensive to study. Yet for some initial conditions the unaveraged solution may be expected to slowly diffuse away from the averaged solution. The averaging principle was first applied to the numerical study of commensurable motion by Schubart (1964, 1968). His method was then used by Giffen (1973) and Froeschlé and Scholl (1974, 1975, 1976, 1977) in their extensive studies of motion at commensurabilities. Even using the averaging method these integrations span no more than 200 000 yr, an amazingly short time considering the age of the solar system.

The mappings I will describe depend on the averaging principle. Their averaged equations of motion are identical to those used by Schubart, Giffen, and Froeschlé and Scholl (except that I retain only terms up to the fourth order in the eccentricities and inclinations). The method of Schubart relies on the averaging principle to justify removing the high-frequency perturbations and the mappings rely on the averaging principle to justify changing the high-frequency perturbations. In each case the assumption is that at least in the first approximation the high-frequency perturbations can be ignored. The initial step, then, in the derivation of the mappings is to analytically average the Hamiltonian to obtain the resonant Hamiltonian.

III. THE RESONANT HAMILTONIAN

In terms of the Poincaré canonical elements (see, e.g., Plummer 1960), the Hamiltonian for a zero-mass test body moving in the field of a large central mass (the Sun) and perturbed by a smaller mass (Jupiter) whose orbit lies outside that of the test body is

$$H = -\frac{\mu_1^2}{2L^2} - \mu R(L, \rho_1, \rho_2, \lambda, \omega_1, \omega_2), \tag{1}$$

where R is the disturbing function, $\mu_1 = 1 - \mu$, and μ is the mass of the secondary. I have chosen units so that the product of the gravitational constant and the sum of the masses is unity and the separation of the two masses is also unity. Following Froeschlé and Scholl, I take $\mu = 1/1047.355$. The Poincaré momenta may be written in terms of the usual osculating elliptic elements:

$$L \equiv (\mu_1 a)^{1/2},$$

$$\rho_1 \equiv (\mu_1 a)^{1/2}[1 - (1 - e^2)^{1/2}] \approx (\mu_1 a)^{1/2} \tfrac{1}{2} e^2,$$

and

$$\rho_2 \equiv [\mu_1 a(1 - e^2)]^{1/2}(1 - \cos i) \approx (\mu_1 a)^{1/2} \tfrac{1}{2} i^2,$$

where a is the semimajor axis, e is the eccentricity, and i is the inclination to the invariable plane. The conjugate coordinates are the mean longitude λ; minus the longitude of periapse, ω_1; and minus the longitude of the ascending node on the invariable plane, ω_2, respectively. The disturbing function may be written as the sum

$$R = \sum_{ijklmn} K^{ijklmn}(L, \rho_1, \rho_2) \times \cos(i\lambda + j\omega_1 + k\omega_2 + l\lambda' + m\omega_1' + n\omega_2'), \tag{2}$$

which is constrained by the requirement that $i - j - k + l - m - n$ be zero and for definiteness i is restricted to be greater than or equal to zero. Jupiter's elements carry a prime. A resonance occurs when one of the cosine arguments is nearly stationary. Since the mean longitudes move much faster than the other angles, this means that $i\dot{\lambda} + l\dot{\lambda}' \approx 0$, or $\dot{\lambda} \approx -l/i \equiv -(i + q)/i$. The integer q is called the order of the resonance; resonance strengths decrease with increasing order since for small e and i their terms in R are proportional to $e^a i^b$, where $a + b = q$. The most important 3/1 resonance terms have $i = 1$ and $q = 2$ and are quadratic in the eccentricities and inclinations. The $i = 2$ resonant terms are smaller by factors quadratic in the eccentricities and inclinations. In this paper all resonant terms with $i \geqslant 2$ are neglected. The terms whose arguments do not involve the mean longitudes, i.e., which have $i = l = 0$, are called secular terms and also affect the motion. In order to construct an algebraic mapping it is necessary to neglect all secular terms that are fourth order or greater in the eccentricities and inclinations. Besides the higher-order 3/1 resonances, there are no neighboring resonances in the range $0.47 < a < 0.49$ with order less than $q = 21$. The largest of these terms is proportional to the 21st power of the eccentricity. It is thus a very good approximation to ignore all nearby resonances. The arguments of all other terms involve nonresonant combinations of the mean longitudes, and rotate at least as fast as the mean longitude of Jupiter. These nonresonant terms will be called high-frequency terms. These high-frequency terms are the terms removed by Schubart's numerical averaging procedure, and the terms which are changed in deriving the mappings.

The explicit form of the disturbing function may be found in, for example, Leverrier (1855), Peirce (1849), or Brouwer and Clemence (1961). In Leverrier's notation,

$$R_{\text{secular}} = (2)^{(0)}\left(\frac{e}{2}\right)^2 + (11)^{(0)}\eta_L^2 + (21)^{(-1)}\left(\frac{e}{2}\right)\left(\frac{e'}{2}\right)\cos(\omega_L - \tilde{\omega}'). \tag{3}$$

The primed quantities belong to Jupiter, $\eta_L^2 \equiv \sin^2 \tfrac{1}{2} J$, where J is the mutual inclination between the orbit of Jupiter and the orbit of the test body, $\tilde{\omega}$ is the longitude of the periapse, and $\omega_L \equiv \tilde{\omega} + \Omega' + \vartheta' - \Omega - \vartheta$, where ϑ and ϑ' are the angles between the ascending nodes of the orbits on the invariable plane and the ascending node of the outer orbit on the inner orbit, and Ω and Ω' are the longitudes of the ascending nodes on the invariable plane. The coefficients are defined as follows:

$$(2)^{(0)} \equiv a\frac{d}{da} b^{(0)}_{1/2}(a) + \tfrac{1}{2} a^2 \frac{d^2}{da^2} b^{(0)}_{1/2}(a), \tag{4}$$

$$(11)^{(0)} \equiv -\tfrac{1}{2} b^{(1)}_{3/2}(a), \tag{5}$$

and

$$(21)^{-1} \equiv 2b^{(1)}_{1/2}(a) - 2a\frac{d}{da} b^{(1)}_{1/2}(a)$$

© American Astronomical Society • Provided by the NASA Astrophysics Data System

1982AJ.....87..577W

$$- a \frac{d^2}{da^2} b^{(1)}_{1/2}(a). \tag{6}$$

The Laplace coefficients $b^{(i)}_j$ are defined by

$$\tfrac{1}{2}\sum b^{(i)}_j(a)\cos i(l'_L - \lambda_L) \equiv \frac{a^{j-1/2}}{[1 - 2a\cos(l'_L - \lambda_L) + a^2]^j}. \tag{7}$$

Similarly,

$$\begin{aligned} R_{\text{resonant}} &= (172)^{(3)}\left(\frac{e}{2}\right)^2 \cos(3l'_L - \lambda_L - 2\omega_L) \\ &+ (182)^{(2)}\left(\frac{e}{2}\right)\left(\frac{e'}{2}\right)\cos(3l'_L - \lambda_L - \omega_L - \tilde{\omega}') \\ &+ (192)^{(1)}\left(\frac{e'}{2}\right)^2 \cos(3l'_L - \lambda_L - 2\tilde{\omega}') \\ &+ (212)^{(3)}\eta_L^2 \cos(3l'_L - \lambda_L - 2\tau'_L), \end{aligned} \tag{8}$$

where l_L is Leverrier's mean longitude, $\lambda_L = l + \tilde{\omega} + \Omega' + \vartheta' - \Omega - \vartheta$, and $\tau_L = \Omega + \vartheta$. The coefficients are

$$(172)^{(3)} \equiv \tfrac{21}{2} b^{(3)}_{1/2}(a) + 5a \frac{d}{da} b^{(3)}_{1/2}(a) + \tfrac{1}{2} a^2 \frac{d^2}{da^2} b^{(3)}_{1/2}(a), \tag{9}$$

$$(182)^{(2)} \equiv -20 b^{(2)}_{1/2}(a) - 10a \frac{d}{da} b^{(2)}_{1/2}(a) - a^2 \frac{d^2}{da^2} b^{(2)}_{1/2}(a), \tag{10}$$

$$(192)^{(1)} \equiv \tfrac{17}{2} b^{(1)}_{1/2}(a) + 5a \frac{d}{da} b^{(1)}_{1/2}(a) + \tfrac{1}{2} a^2 \frac{d^2}{da^2} b^{(1)}_{1/2}(a) - \tfrac{27}{2} a, \tag{11}$$

and

$$(212)^{(3)} = \tfrac{1}{2} b^{(2)}_{3/2}(a). \tag{12}$$

The coefficient $(192)^{(1)}$ has been corrected to include the indirect contribution (see Leverrier 1855). The coefficients vary little over the very small range of semimajor axes of the 3/1 Kirkwood gap so I simply evaluate them at exact resonance. In all terms not involving the mutual inclination, each $\Omega + \vartheta$ is cancelled by an $\Omega' + \vartheta'$ since they differ only by terms of order J^2. The terms involving the mutual inclination, J, must be written in terms of the individual inclinations and nodes. To order J^2 (see Plummer 1960),

$$\eta_L^2 \equiv \sin^2\frac{J}{2} = \left(\frac{i}{2}\right)^2 + \left(\frac{i'}{2}\right)^2 - 2\left(\frac{i}{2}\right)\left(\frac{i'}{2}\right)\cos(\Omega' - \Omega) \tag{13}$$

and

$$\begin{aligned} \eta^2\cos(3l'_L - \lambda_L - 2\tau_L) &= \left(\frac{i}{2}\right)^2 \cos[3(l' + \tilde{\omega}') - (l + \tilde{\omega}) - 2\Omega] - 2\left(\frac{i}{2}\right)\left(\frac{i'}{2}\right) \\ &\times \cos[3(l' + \tilde{\omega}') - (l + \tilde{\omega}) - (\Omega + \Omega')] + \left(\frac{i'}{2}\right)^2 \cos[3(l' + \tilde{\omega}') - (l + \tilde{\omega}) - 2\Omega']. \end{aligned} \tag{14}$$

The disturbing function can now be written in terms of the canonical Poincaré elements:

$$\mu R_{\text{secular}} = -F_1 2\rho_1 - e'\bar{F}_1(2\rho_1)^{1/2}\cos(\omega_1 + \tilde{\omega}') - F_2 2\rho_2 - i'\bar{F}_2(2\rho_2)^{1/2}\cos(\omega_2 + \Omega') \tag{15}$$

and

$$\begin{aligned} \mu R_{\text{resonant}} &= C_1 2\rho_1 \cos(3t - \lambda + 2\omega_1) + e'D_1(2\rho_1)^{1/2}\cos(3t - \lambda + \omega_1 - \tilde{\omega}') + e'^2 E_1 \cos(3t - \lambda - 2\tilde{\omega}') \\ &+ C_2 2\rho_2 \cos(3t - \lambda + 2\omega_2) + i'D_2(2\rho_2)^{1/2}\cos(3t - \lambda + \omega_2 - \Omega') + i'^2 E_2 \cos(3t - \lambda - 2\Omega'), \end{aligned} \tag{16}$$

where the coefficients are

$$F_1 \equiv -\frac{\mu(2)^{(0)}}{4(\mu_1 a_{1/3})^{1/2}} \approx -0.205\,069\,4\,\mu, \tag{17}$$

$$\bar{F}_1 \equiv -\frac{\mu(21)^{(-1)}}{4(\mu_1 a_{1/3})^{1/4}} \approx 0.198\,705\,4\,\mu, \tag{18}$$

$$F_2 \equiv -\frac{\mu(11)^{(0)}}{4(\mu_1 a_{1/3})^{1/2}} \approx 0.426\,697\,3\,\mu, \tag{19}$$

$$\bar{F}_2 \equiv \frac{\mu(11)^{(0)}}{2(\mu_1 a_{1/3})^{1/4}} \approx -0.710\,381\,2\,\mu, \tag{20}$$

$$C_1 \equiv \frac{\mu(172)^{(3)}}{4(\mu_1 a_{1/3})^{1/2}} \approx 0.863\,157\,9\,\mu, \tag{21}$$

© American Astronomical Society • Provided by the NASA Astrophysics Data System

1982AJ.....87..577W

$$D_1 \equiv \frac{\mu(182)^{(2)}}{4(\mu_1 a_{1/3})^{1/4}} \approx -2.656\,407\,\mu, \tag{22}$$

$$E_1 \equiv \frac{\mu(192)^{(1)}}{4} \approx 0.362\,953\,6\,\mu, \tag{23}$$

$$C_2 \equiv \frac{\mu(212)^{(3)}}{4(\mu_1 a_{1/3})^{1/2}} \approx 0.248\,346\,1\,\mu, \tag{24}$$

$$D_2 \equiv -\frac{\mu(212)^{(3)}}{2(\mu_1 a_{1/3})^{1/4}} \approx -0.413\,455\,6\,\mu, \tag{25}$$

$$E_2 \equiv -\frac{\mu(212)^{(3)}}{4} \approx 0.172\,083\,9\,\mu. \tag{26}$$

The resonant Hamiltonian is of the form

$$H_R = -\frac{\mu_1^2}{2L^2} - \mu R_{\text{secular}}(\omega_1, \rho_1, \omega_2, \rho_2) - \mu R_{\text{resonant}}(\omega_1, \rho_1, \omega_2, \rho_2, 3t - \lambda). \tag{27}$$

In order to remove the explicit time dependence from Eq. (27),* I perform a canonical transformation to the coordinate $\varphi = 3t - \lambda$ via the time-dependent generating function $F = (3t - \lambda)(\Phi + L_R) + \omega_1 \rho_1' + \omega_2 \rho_2'$, where for convenience I have also translated the origin of momentum to be the exact resonance. $L_R \equiv (\mu_1 a_{1/3})^{1/2}$ is defined so that $\mu = \partial H_R'/\partial \Phi$ is zero at $\Phi = 0$. This gives $L_R = (\frac{1}{3}\mu_1^2)^{1/3}$. Keeping only the quadratic term in Φ the resonant Hamiltonian is now

$$H_R = \tfrac{1}{2}\alpha\Phi^2 - \mu R_{\text{secular}}(\omega_1, \rho_1, \omega_2, \rho_2) - \mu R_{\text{resonant}}(\omega_1, \rho_1, \omega_2, \rho_2, \varphi), \tag{28}$$

where

$$\alpha = \left.\frac{\partial^2 H_R}{\partial \Phi^2}\right|_{\Phi=0} = -\frac{3\mu_1^2}{L_R^4} \approx -12.988\,51 \tag{29}$$

and I have dropped the primes.

Finally the eccentricity and inclination of Jupiter must be specified. Brouwer and van Woerkom (1950) provide a solution to the secular problem of planetary motion. The elements of Jupiter's orbit are given in the form of sums:

$$\sum_k c_k \cos(-s_k t + \delta_k) = e' \cos\tilde{\omega}' \equiv \xi_1, \tag{30}$$

$$\sum_k c_k \sin(-s_k t + \delta_k) = e' \sin\tilde{\omega}' \equiv \eta_1, \tag{31}$$

$$\sum_k d_k \cos(-s_k' t + \delta_k') = i' \cos\Omega' \equiv \xi_2, \tag{32}$$

$$\sum_k d_k \sin(-s_k' t + \delta_k') = i' \sin\Omega' \equiv \eta_2. \tag{33}$$

Two of the c_k dominate all the others, and I include only those terms. The values are $c_1 = 0.044\,818\,8$, $c_2 = 0.015\,354\,6$, $s_1 = -3.977\,69 \times 10^{-5}$, $s_2 = -2.571\,67 \times 10^{-4}$. It is necessary to include three of the d_k: $d_1 = 0.006\,306\,4$, $d_2 = 0.000\,957\,1$, $d_3 = 0.001\,168\,9$, $s_1' = 2.382\,736 \times 10^{-4}$, $s_2' = 2.687\,651 \times 10^{-5}$, and $s_3' = 6.273\,352 \times 10^{-6}$.

In terms of the canonical momenta $x_i \equiv (2\rho_i)^{1/2}\cos\omega_i$ and their canonical coordinates $y_i \equiv (2\rho_i)^{1/2}\sin\omega_i$, the final form of the resonant Hamiltonian is

$$\begin{aligned} H_R = {} & \tfrac{1}{2}a\Phi^2 + \mu F_1(x_1^2 + y_1^2) + \mu\bar{F}_1(x_1\xi_1 - y_1\eta_1) + \mu F_2(x_2^2 + y_2^2) + \mu\bar{F}_2(x_2\xi_2 - y_2\eta_2) \\ & - \mu[C_1(x_1^2 - y_1^2) + \mu D_1(x_1\xi_1 + y_1\eta_1) + E_1(\xi_1^2 - \eta_1^2)]\cos\varphi \\ & - \mu[C_1 2x_1 y_1 - D_1(x_1\eta_1 - y_1\xi_1) - E_1 2\xi_1\eta_1]\sin\varphi \\ & - \mu[C_2(x_2^2 - y_2^2) + D_2(x_2\xi_2 + y_2\eta_2) + E_2(\xi_2^2 - \eta_2^2)]\cos\varphi \\ & - \mu[C_2 2x_2 y_2 - D_2(x_2\eta_2 - y_2\xi_2) - E_2 2\xi_2\eta_2]\sin\varphi. \end{aligned} \tag{34}$$

*The resonant Hamiltonian still contains the explicit time dependence of Jupiter's elements.

© American Astronomical Society • Provided by the NASA Astrophysics Data System

1982AJ.....87..577W

The resonant Hamiltonian for the planar-elliptic problem can be obtained from the full resonant Hamiltonian, Eq. (34), by setting the coefficients of all terms involving the inclinations to zero and fixing Jupiter's orbit by setting $\xi_1 = e_J$ and $\eta_1 = 0$. e_J is the constant value of Jupiter's eccentricity. The resulting resonant Hamiltonian is

$$H'_R = \tfrac{1}{2}\alpha\Phi^2 + F_1(x_1^2 + y_1^2) + \bar{F}_1 e_J x_1 - [C_1(x_1^2 - y_1^2) + D_1 e_J x_1 + E_1 e_J^2]\cos\varphi - [C_1 2x_1 y_1 + D_1 y_1 e_J]\sin\varphi. \tag{35}$$

IV. PLANAR-ELLIPTIC MAPPING

The resonant Hamiltonian was derived in Sec. III by analytically removing the high-frequency terms in the disturbing function. These high-frequency terms are the same terms that are removed numerically by Schubart's averaging procedure. Their removal is justified by the averaging principle, which argues that the high-frequency terms contribute only periodic variations about the motion determined by the resonant Hamiltonian. If the high-frequency terms can be removed without qualitatively affecting the evolution, they can also be modified. This is exactly what will be done to derive the mappings. The mappings thus bear the same relation to the unaveraged equations of motion as the numerically averaged equations used by Schubart, Giffen, and Froeschlé and Scholl. Each one differs from the real equations of motion by high-frequency terms. In the planar-elliptic case the mappings are perhaps even closer to the original problem than Schubart's method. In Schubart's method the number of degrees of freedom is reduced to 2, thus eliminating the possibility of Arnol'd diffusion. The mappings retain high-frequency terms, albeit incorrect ones, and diffusion remains a possibility as in the actual problem.

In this section, then, I derive a mapping for the planar-elliptic problem, starting from the resonant Hamiltonian H'_R given in Eq. (35). To H'_R I add new high-frequency terms,

$$\begin{aligned} H' = {} & \tfrac{1}{2}\alpha\Phi^2 + F_1(x_1^2 + y_1^2) + \bar{F}_1 e_J x_1 - \sum_{i=-\infty}^{\infty} C_1(x_1^2 - y_1^2)\cos[\varphi - i\Omega(t - \zeta_1)] \\ & - \sum_{i=-\infty}^{\infty} D_1 e_J x_1 \cos[\varphi - i\Omega(t - \zeta_2)] - \sum_{i=-\infty}^{\infty} E_1 e_J^2 \cos[\varphi - i\Omega(t - \zeta_3)] \\ & + \sum_{i=-\infty}^{\infty} C_1 2x_1 y_1 \cos\left[\varphi - \tfrac{1}{2}\pi - i\Omega(t - \gamma_1)\right] + \sum_{i=-\infty}^{\infty} D_1 e_J x_1 \cos\left[\varphi - \tfrac{1}{2}\pi - i\Omega(t - \gamma_2)\right]. \end{aligned} \tag{36}$$

The frequency Ω is the same as Jupiter's mean motion when $\Omega = 1$, but for the time being it will be left as a parameter. These high-frequency terms are of the same form as the real high-frequency terms that were originally removed, but are chosen so that each sum becomes a sum of delta functions. Consider just the first sum:

$$\begin{aligned} \sum_{i=-\infty}^{\infty} \cos[\varphi - i\Omega(t - \zeta_1)] &= (\cos\varphi)\sum_{i=-\infty}^{\infty} \cos[i\Omega(t - \zeta_1)] \\ &= (\cos\varphi)\sum_{i=-\infty}^{\infty} 2\pi\delta[\Omega(t - \zeta_1) - 2\pi i] \\ &\equiv (\cos\varphi)2\pi\delta_{2\pi}[\Omega(t - \zeta_1)]. \end{aligned} \tag{37}$$

The second equality follows from the well-known Fourier transform of a delta function and the last equality implicitly defines $\delta_{2\pi}$ as a periodic delta function with period 2π.

Thus the planar-elliptic mapping Hamiltonian becomes

$$\begin{aligned} H' = {} & \tfrac{1}{2}\alpha\Phi^2 + F_1(x_1^2 + y_1^2) + \bar{F}_1 e_J x_1 - C_1(x_1^2 - y_1^2)(\cos\varphi)2\pi\delta_{2\pi}[\Omega(t - \zeta_1)] \\ & - D_1 e_J x_1 (\cos\varphi)2\pi\delta_{2\pi}[\Omega(t - \zeta_2)] - E_1 e_J^2 (\cos\varphi)2\pi\delta_{2\pi}[\Omega(t - \zeta_1)] \\ & - C_1 2x_1 y_1 (\sin\varphi)2\pi\delta_{2\pi}[\Omega(t - \gamma_1)] - D_1 e_J y_1 (\sin\varphi)2\pi\delta_{2\pi}[\Omega(t - \gamma_2)]. \end{aligned} \tag{38}$$

The constants ζ_i and γ_i determine the times at which the delta functions act and are arbitrary. I choose $0 \leqslant \zeta_1 < \zeta_2 < \zeta_3$, $\pi/2\Omega \leqslant \gamma_1 < \gamma_2$ and let $\zeta_3 \to 0$ and $\gamma_2 \to \pi/2\Omega$. The delta functions thus all act at either $t = 0$ or $t = \pi/2\Omega$, but they have a definite ordering. This ordering is a matter of choice and is certainly not the only one possible, nor even necessarily the best. Between the delta functions the motion is determined entirely by the secular terms

$$H_{\text{secular}} = \tfrac{1}{2}\alpha^2 + F_1(x_1^2 + y_1^2) + \bar{F}_1 e_J x_1. \tag{39}$$

This Hamiltonian has the trivial solution

$$x_1 = x_1(t_0)\cos[2F_1(t - t_0)] - y_1(t_0)\sin[2F_1(t - t_0)] - (\bar{F}/2F)\{1 - \cos[2F(t - t_0)]\}, \tag{40}$$

$$y_1 = x_1(t_0)\sin[2F_1(t - t_0)] + y_1(t_0)\cos[2F_1(t - t_0)] + (\bar{F}/2F)\sin[2F(t - t_0)], \tag{41}$$

© American Astronomical Society • Provided by the NASA Astrophysics Data System

1982AJ.....87..577W

$$\Phi = \Phi(t_0), \tag{42}$$

and

$$\varphi = \alpha\Phi_0(t - t_0) + \varphi_0. \tag{43}$$

To integrate across the delta functions I use a limiting procedure; the delta functions are replaced by

$$\delta(t - t_i) \leftarrow \lim_{\Delta \to 0} \begin{cases} 1/\Delta, & t_j \leqslant t < t_1 + \Delta \\ 0, & \text{otherwise} \end{cases}. \tag{44}$$

Each delta function is integrated in turn. The Hamiltonian during the first delta function is

$$H_1 = -\frac{2\pi C_1}{\Delta\Omega}(x_1^2 - y_1^2)\cos\varphi, \tag{45}$$

which leads to the equations of motion

$$\dot{x}_1 = -\frac{\partial H}{\partial y_1} = -\frac{4\pi C_1}{\Delta\Omega} y_1 \cos\varphi \equiv -\frac{R_1}{\Delta} y_1, \tag{46}$$

$$\dot{y}_1 = \frac{\partial H}{\partial x_1} = -\frac{4\pi C_1}{\Delta\Omega} x_1 \cos\varphi \equiv -\frac{R_1}{\Delta} x_1, \tag{47}$$

$$\dot{\Phi} = -\frac{2\pi C_1}{\Delta\Omega}(x_1^2 - y_1^2)\sin\varphi, \tag{48}$$

and

$$\dot{\varphi} = 0. \tag{49}$$

The solutions to the first two of these equations are

$$x_1(t) = x_1(t_1)\cosh\left(\frac{R_1(t - t_1)}{\Delta}\right) - y_1(t_1)\sinh\left(\frac{R_1(t - t_1)}{\Delta}\right) \tag{50}$$

and

$$y_1(t) = y_1(t_1)\cosh\left(\frac{R_1(t - t_1)}{\Delta}\right) - x_1(t_1)\sinh\left(\frac{R_1(t - t_1)}{\Delta}\right). \tag{51}$$

The changes in x_1 and y_1 across the first delta function are then calculated by setting $t = t_1 + \Delta$ (and letting Δ go to zero). They are

$$\Delta x_1 = x_1(t_1)\left[\cosh\left(\frac{4\pi C_1}{\Omega}\cos\varphi\right) - 1\right] - y_1(t_1)\sinh\left(\frac{4\pi C_1}{\Omega}\cos\varphi\right) \tag{52}$$

and

$$\Delta y_1 = y_1(t_1)\left[\cosh\left(\frac{4\pi C_1}{\Omega}\cos\varphi\right) - 1\right] - x_1(t_1)\sinh\left(\frac{4\pi C_1}{\Omega}\cos\varphi\right). \tag{53}$$

Having solved for $x_1(t)$ and $y_1(t)$, the equation for Φ becomes

$$\dot{\Phi} = -\frac{2\pi C_1}{\Delta\Omega}[x_1^2(t) - y_1^2(t)]\sin\varphi(t_1) = -\frac{2\pi C_1}{\Delta\Omega}[x_1^2(t_1) - y_1^2(t_1)]\sin\varphi(t_1), \tag{54}$$

which yields for the change in Φ across the delta function

$$\Delta\Phi = -\frac{2\pi C_1}{\Delta\Omega}[x_1^2(t_1) - y_1^2(t_1)]\sin\varphi(t_1). \tag{55}$$

The Hamiltonian during the second delta function is

$$H_2 = -\frac{2\pi D_1}{\Delta\Omega} e_J x_1 \cos\varphi(t_2). \tag{56}$$

The equations of motion are

$$\dot{x}_1 = 0, \tag{57}$$

$$\dot{y}_1 = -\frac{2\pi D_1}{\Delta\Omega} e_J \cos\varphi(t_2), \tag{58}$$

$$\dot{\Phi} = -\frac{2\pi D_1}{\Delta\Omega} e_J x_1 \sin\varphi(t_2), \tag{59}$$

and

$$\dot{\varphi} = 0. \tag{60}$$

The changes in y_1 and Φ across the second delta function are

$$\Delta y_1 = -\frac{2\pi D_1}{\Omega} e_J \cos\varphi(t_2), \tag{61}$$

$$\Delta\Phi = -\frac{2\pi D_1}{\Omega} e_J x_1(t_2)\sin\varphi(t_2). \tag{62}$$

Only Φ changes across the third delta function. The change is

$$\Delta\Phi = -\frac{2\pi E_1}{\Omega} e_J^2 \sin\varphi(t_3). \tag{63}$$

During the fourth delta function the Hamiltonian is

$$H_4 = -\frac{4\pi C_1}{\Delta\Omega} x_1 y_1 \sin\varphi(t_4). \tag{64}$$

The equations of motion are

$$\dot{x}_1 = \frac{4\pi C_1}{\Delta\Omega} x_1 \sin\varphi(t_4), \tag{65}$$

$$\dot{y}_1 = -\frac{4\pi C_1}{\Delta\Omega} y_1 \sin\varphi(t_4), \tag{66}$$

and

$$\dot{\Phi} = \frac{4\pi C_1}{\Delta\Omega} x_1 y_1 \cos\varphi(t_4). \tag{67}$$

Their solutions are

$$x_1(t) = x_1(t_4)\exp\left(\frac{4\pi t_1 \sin\varphi(t_4)}{\Delta\Omega}(t - t_4)\right), \tag{68}$$

$$y_1(t) = y_1(t_4)\exp\left(\frac{4\pi t_1 \sin\varphi(t_4)}{\Delta\Omega}(t - t_4)\right), \tag{69}$$

and

$$\Phi(t) = \Phi(t_4) + (t - t_4)\frac{4\pi C_1}{\Delta\Omega}\cos\varphi(t_4). \tag{70}$$

© American Astronomical Society • Provided by the NASA Astrophysics Data System

1982AJ.....87..577W

The changes across the fourth delta function are then

$$\Delta x_1 = x_1(t_4)\left[\exp\left(\frac{4\pi C_1 \sin\varphi(t_4)}{\Omega} \right) - 1 \right], \tag{71}$$

$$\Delta y_1 = y_1(t_4)\left[\exp\left(\frac{4\pi C_1 \sin\varphi(t_4)}{\Omega} \right) - 1 \right], \tag{72}$$

and

$$\Delta\Phi = \frac{4\pi C_1}{\Omega} x_1(t_4) y_1(t_4) \cos\varphi(t_4). \tag{73}$$

The changes across the fifth delta function are evaluated in exactly the same manner. They are

$$\Delta x_1 = \frac{2\pi D_1}{\Omega} e_J \sin\varphi(t_5), \tag{74}$$

$$\Delta\Phi = \frac{2\pi D_1}{\Omega} e_J y_1(t_5) \cos\varphi(t_5). \tag{75}$$

The planar-elliptic mapping is now complete. For clarity I will review one complete cycle of the mapping, starting at $t = 0$ and ending at $t = 2\pi/\Omega$. Initially the elements are $x_1^{(0)}, y_1^{(0)}, \Phi^{(0)}$, and $\varphi^{(0)}$. There are seven steps:

Step 1

$$x_1^{(1)} = x_1^{(0)} \cosh\left(\frac{4\pi C_1}{\Omega} \cos\varphi^{(0)} \right) - y_1^{(0)} \sinh\left(\frac{4\pi C_1}{\Omega} \cos\varphi^{(0)} \right), \tag{76}$$

$$y_1^{(1)} = y_1^{(0)} \cosh\left(\frac{4\pi C_1}{\Omega} \cos\varphi^{(0)} \right) - x_1^{(0)} \sinh\left(\frac{4\pi C_1}{\Omega} \cos\varphi^{(0)} \right), \tag{77}$$

$$\Phi^{(1)} = \Phi^{(0)} - \frac{2\pi C_1}{\Omega} [(x_1^{(0)})^2 - (y_1^{(0)})^2] \sin\varphi^{(0)}, \tag{78}$$

$$\varphi^{(1)} = \varphi^{(0)}; \tag{79}$$

Step 2

$$x_1^{(2)} = x_1^{(1)}, \tag{80}$$

$$y_1^{(2)} = y_1^{(1)} - \frac{2\pi D_1}{\Omega} e_J \cos\varphi^{(1)}, \tag{81}$$

$$\Phi^{(2)} = \Phi^{(1)} - \frac{2\pi D_1}{\Omega} e_J x_1^{(1)} \sin\varphi^{(1)}, \tag{82}$$

$$\varphi^{(2)} = \varphi^{(1)}; \tag{83}$$

Step 3

$$x_1^{(3)} = x_1^{(2)}, \tag{84}$$

$$y_1^{(3)} = y_1^{(2)}, \tag{85}$$

$$\Phi^{(3)} = \Phi^{(2)} - \frac{2\pi E_1}{\Omega} e_J^2 \sin\varphi^{(2)}, \tag{86}$$

$$\varphi^{(3)} = \varphi^{(2)}; \tag{87}$$

Step 4

$$x_1^{(4)} = x_1^{(3)} \cos\frac{\pi F}{\Omega} - y_1^{(3)} \sin\frac{\pi F}{\Omega} - \frac{\bar{F}}{2F}\left(1 - \cos\frac{\pi F}{\Omega}\right), \tag{88}$$

$$y_1^{(4)} = x_1^{(3)} \sin\frac{\pi F}{\Omega} + y_1^{(3)} \cos\frac{\pi F}{\Omega} + \frac{\bar{F}}{2F} \sin\frac{\pi F}{\Omega}, \tag{89}$$

$$\Phi^{(4)} = \Phi^{(3)}, \tag{90}$$

$$\varphi^{(4)} = \varphi^{(3)} + (\pi\alpha/2\Omega)\Phi^{(3)}; \tag{91}$$

Step 5

$$x_1^{(5)} = x_1^{(4)} \exp\left(\frac{4\pi C_1}{\Omega} \sin\varphi^{(4)} \right), \tag{92}$$

$$y_1^{(5)} = y_1^{(4)} \exp\left(-\frac{4\pi C_1}{\Omega} \sin\varphi^{(4)} \right), \tag{93}$$

$$\Phi^{(5)} = \Phi^{(4)} + \frac{4\pi C_1}{\Omega} x_1^{(4)} y_1^{(4)} \cos\varphi^{(4)}, \tag{94}$$

$$\varphi^{(5)} = \varphi^{(4)}; \tag{95}$$

Step 6

$$x_1^{(6)} = x_1^{(5)} + \frac{2\pi D_1}{\Omega} e_J \sin\varphi^{(5)}, \tag{96}$$

$$y_1^{(6)} = y_1^{(5)}, \tag{97}$$

$$\Phi^{(6)} = \Phi^{(5)} + \frac{2\pi D_1}{\Omega} e_J y_1^{(5)} \cos\varphi^{(5)}, \tag{98}$$

$$\varphi^{(6)} = \varphi^{(5)}; \tag{99}$$

Step 7

$$x_1^{(7)} = x_1^{(6)} \cos\frac{3\pi F}{\Omega} - y_1^{(6)} \sin\frac{3\pi F}{\Omega} - \frac{\bar{F}}{2F}\left(1 - \cos\frac{3\pi F}{\Omega}\right), \tag{100}$$

$$y_1^{(7)} = x_1^{(6)} \sin\frac{3\pi F}{\Omega} + y_1^{(6)} \cos\frac{3\pi F}{\Omega} + \frac{\bar{F}}{2F} \sin\frac{3\pi F}{\Omega}, \tag{101}$$

$$\Phi^{(7)} = \Phi^{(6)}, \tag{102}$$

$$\varphi^{(7)} = \varphi^{(6)} + \frac{3\pi\alpha}{2\Omega} \Phi^{(6)}. \tag{103}$$

These seven steps constitute one iteration of the mapping. In Sec. V, I present the results of some calculations using this planar-elliptic mapping.

V. PLANAR-ELLIPTIC MAPPING CALCULATIONS

Primarily as a test of the mapping I redid the work of Scholl and Froeschlé (1974). They study the range of variation of the orbital elements for a large number of initial conditions near the 3/1 resonance and the mapping gave variations in the eccentricities and semimajor axes which were in most cases very close to their results. The differences arise for several reasons. First, Scholl and Froeschlé do not specify exactly the initial condi-

© American Astronomical Society • Provided by the NASA Astrophysics Data System

1982AJ.....87..577W

tions used nor the length of each integration. Some of their orbits were integrated for 12 000 yr, while others were integrated for 50 000 yr. There were no qualitative differences in the variations over the two time intervals so the times were not specified. A more fundamental reason is that nearby orbits in the "ergodic" region separate at an exponential rate, so any small initial error quickly manifests itself. Because of the presence of the high-frequency terms there is an inherent ambiguity about what starting values for the mapping correspond to the initial conditions of the averaged differential equations. In the "ergodic" region this uncertainty grows exponentially. An exact comparison of the two can be expected only in the quasiperiodic region of phase space, i.e., either for small eccentricities (<0.1) near the resonance or outside the resonance region. Finally, when the variation in the eccentricity is large (>0.3), the mapping can be only qualitatively correct because of the truncation of the disturbing function to the second-order terms in the eccentricities.

In order to aid my comparison of the mapping and the averaged differential equations, Scholl and Froeschlé kindly provided the details of several orbits. Figure 1 shows a plot of the eccentricity versus time for one of these orbits, with $\Phi(t=0)=0$, $\varphi(t=0)=\pi$, $y_1(t=0)=0$, and $e(t=0)=0.05$. For this calculation e_J was chosen to be 0.048. Even though this orbit is started at exact resonance, it looks remarkably regular. From the appearance of a surface of section, one would conclude that this orbit is quasiperiodic. This is an example of the low-eccentricity orbits that Greenberg and Scholl describe as behaving "nonresonantly." The integration step was three years with a relative accuracy per integration step of 10^{-12}. The calculation took 40 min on an IBM 360. Next comes the real surprise. Figure 2

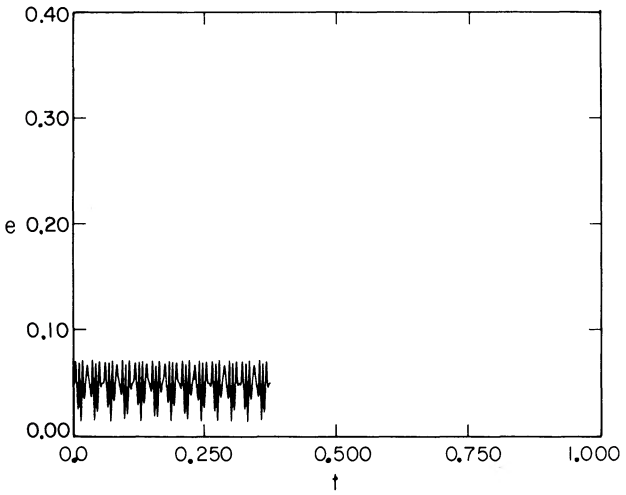

FIG. 1. Eccentricity vs time using the averaged differential equations (in the planar-elliptic approximation) for the initial conditions $\Phi=0$, $\varphi=\pi$, $y_1=0$, and $e=0.05$. Here t is measured in units of $20\,000T_J \approx 240\,000$ yr, where T_J is Jupiter's period.

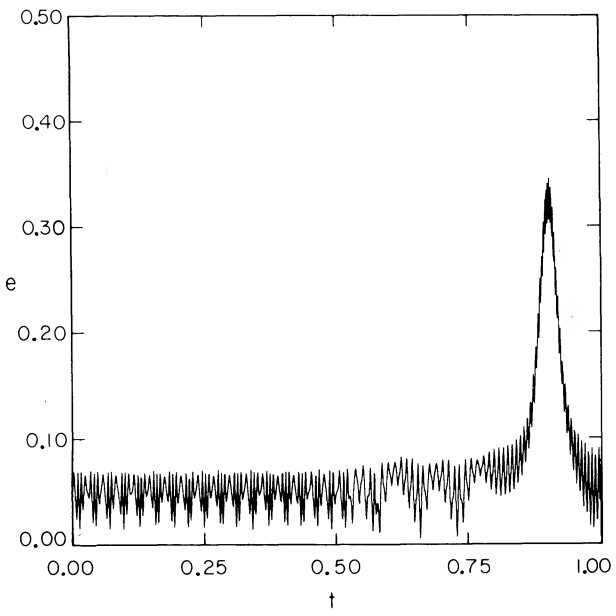

FIG. 2. Eccentricity vs time using the planar-elliptic mapping for the same initial conditions as in Fig. 1. As in Fig. 1 the time is measured in units of $20\,000T_J \approx 240\,000$ yr.

shows the results of the mapping (with $\Omega = 1/2$) for the same initial conditions. For the first 100 000 yr the mapping reproduces quite closely the very regular motion of Fig. 1. The eccentricity then noticeably becomes more irregular and after nearly 240 000 yr a huge spike occurs. This mapping "integration" was calculated in double precision (eight 8-bit bytes) on the Caltech IBM 370/3032. The calculation took only a couple of seconds. Naturally one wonders if this jump could somehow be due to an accumulation of roundoff error. In order to check this the calculation was repeated in quadruple precision (16 8-bit bytes). Of course, the orbits differed slightly but the eccentricity plots were indistinguishable. The jump still occurs, and at exactly the same time. What causes the jump? Is the jump an artifact of my special choice of high-frequency terms or would a similar jump occur in the real unaveraged problem? The underlying philosophy of this work is that high-frequency perturbations generally can be ignored. Their presence is important, though, because they permit a slow diffusion. Because of the diffusive character of this instability, the exact form of the high-frequency perturbations is unimportant. At least in the first approximation it is primarily just their frequency which will determine the rate of diffusion.

In order to help isolate the effect of the high frequencies in the planar-elliptic mapping, I studied the evolution of this same orbit with several different mapping frequencies Ω. The times to first jump, T_{jump}, are shown in Fig. 3. As the mapping frequency gets higher, the time to first jump gets longer. On a logarithmic scale the relationship between T_{jump} and Ω appears almost linear.

© American Astronomical Society • Provided by the NASA Astrophysics Data System

1982AJ.....87..577W

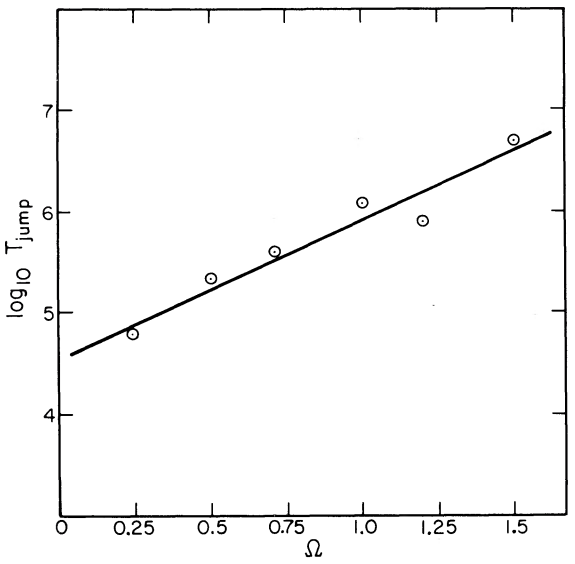

FIG. 3. The times to first jump (in years) plotted vs the mapping frequency Ω. The initial conditions are the same as Figs. 1 and 2. Jupiter's actual frequency corresponds to $\Omega = 1$.

One possible explanation of this is that the trajectories undergo a slow diffusion until they get to a point where jumps occur. If the diffusion rate depends exponentially on the high frequency, i.e.,

$$D \propto \exp(-\alpha\Omega) \tag{104}$$

and the distance in phase space that must be covered in order to get the jump is Δx, then the time to first jump would obey the simple diffusion law

$$\Delta x = DT_{\text{jump}}^2 \propto e^{-\alpha\Omega} T_{\text{jump}}^2, \tag{105}$$

which gives

$$T_{\text{jump}} \propto (\Delta x)^{1/2} e^{\alpha\Omega/2}. \tag{106}$$

The line in Fig. 3 is a linear least-squares fit of the above expression (with $\alpha = 6.27$). It thus seems possible that diffusion is present, but it is certainly not proved. It is also interesting to see how this behavior is affected by varying Jupiter's eccentricity. The principal effect is that the height of the spike changes. Figure 4 shows the results. Finally, I verified that qualitatively the same results are obtained for several different choices of the arbitrary phases ξ_i and γ_i in Eq. (38).

The fact that this orbit undergoes such an extremely large increase in eccentricity introduces a new possibility for the origin of the 3/1 Kirkwood gap. Taking into account the secular variations of Mars' orbit, an asteroid at the 3/1 commensurability need only have an eccentricity of 0.3 to be a Mars crosser. If large eccentricity increases are typical for orbits near the 3/1 commensurability, it is possible that the gap was cleared by close encounters with Mars. The first step in evaluating this hypothesis is to find out how typical it is for orbits near the commensurability to cross the orbit of Mars and to see if the removal of these Mars crossers could account for the gap. Eventually it will be necessary to estimate lifetimes for the asteroids and check that they are consistent with what is known about the collision history of Mars, but this is beyond the scope of this paper. To test the hypothesis, I "integrated" with the mapping a sample distribution of 300 test asteroids with initial conditions in the neighborhood of the 3/1 commensurability for two million years each. In order to get a distribution that would simulate the real asteroid distribution without a gap, I took the elements of the first 300 asteroids in the TRIAD file with $e < 0.3$ and with semimajor axes between 0.49 and 0.52 and shifted their semimajor axes so that they ranged from 0.4725 to 0.4875. The resulting distribution of eccentricities and semimajor axes is shown in Fig. 5. Since the mapping frequency does not seem to affect the motion except to change the rate of diffusion, I used the relatively small mapping frequency of $\Omega = 1/4$ to speed up any diffusion. I also set Jupiter's eccentricity to its maximum, $e_J = 0.060\ 173\ 4$ (see Plummer 1960). Figure 6 shows the initial conditions of those test asteroids that did not reach an eccentricity of 0.3 in two million years, i.e., it is the same as Fig. 5 but with the Mars crossers removed. It is clear that a definite gap has been formed. It should be mentioned that perhaps 60% of those test asteroids that became Mars crossing did so within the first 50 000 yr. Froeschlé and Scholl did not identify this process even though it is consistent with their results. The great advantage of the mapping is that many more initial conditions could be studied. It seems probable that even without diffusion at least some of the gap can be attributed to this mechanism of close encounters with Mars.

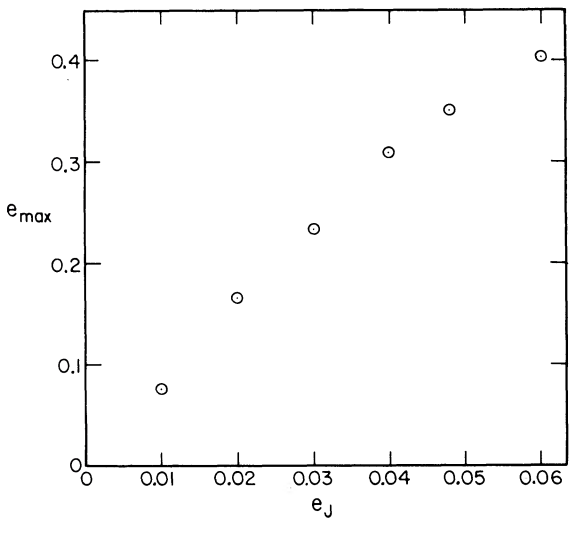

FIG. 4. The height of the jump in eccentricity vs the value given to Jupiter's eccentricity e_J. Froeschlé and Scholl use $e_J = 0.048$. Jupiter has a maximum eccentricity of 0.060 173 4.

© American Astronomical Society • Provided by the NASA Astrophysics Data System

1982AJ.....87..577W

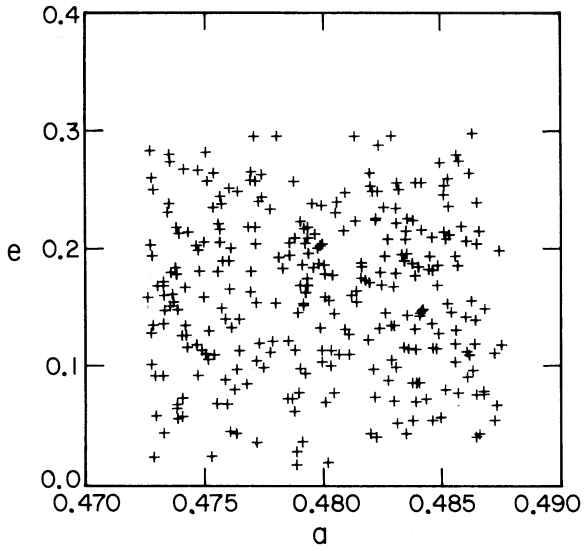

FIG. 5. The eccentricities vs semimajor axes for the 300 test asteroids of the distribution.

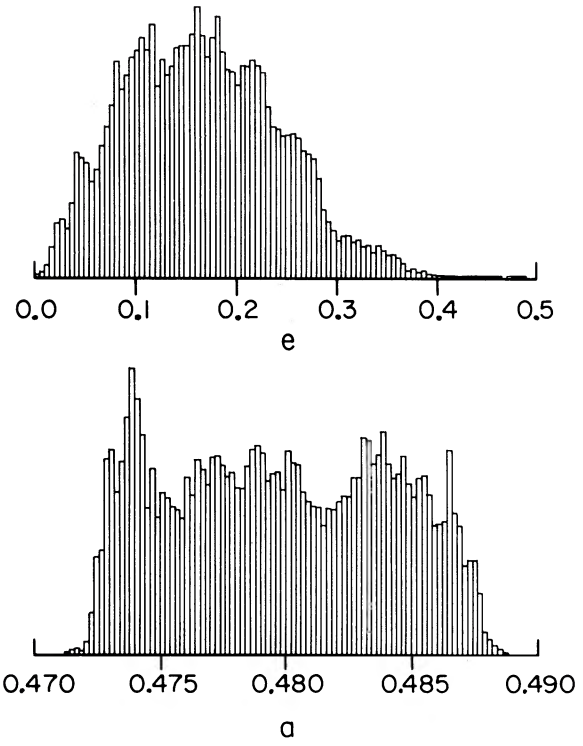

FIG. 7. Histograms of the eccentricities and semimajor axes averaged over 5000 yr for the full distribution of initial conditions.

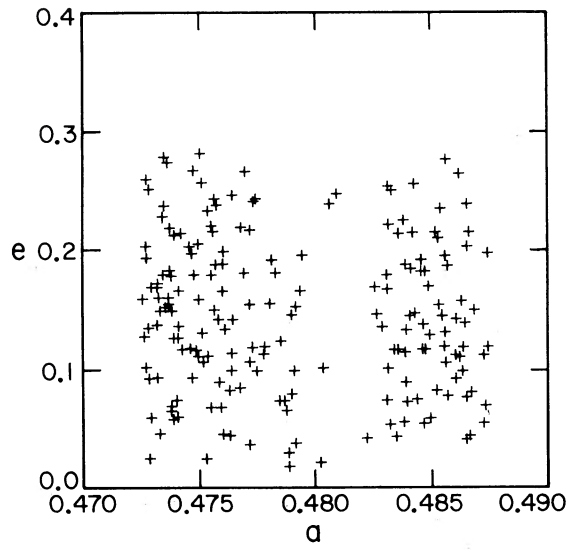

FIG. 6. Same as Fig. 5, but with the initial conditions of those test asteroids that became Mars crossers in two million years removed.

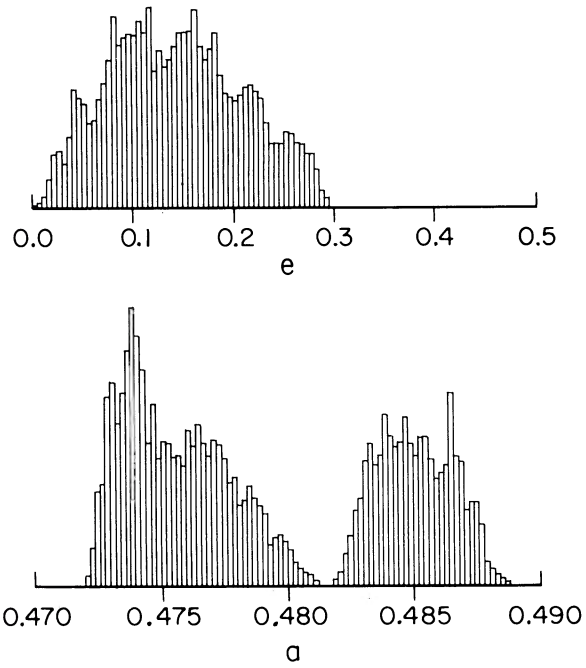

FIG. 8. Histograms of the averaged eccentricities and semimajor axes for those test asteroids that did not become Mars crossers in two million years.

© American Astronomical Society • Provided by the NASA Astrophysics Data System

1982AJ.....87..577W

Note that no secular drift of semimajor axes could be detected. Figures 5 and 6 are snapshots in time of the distribution. To see what these distributions look like when averaged over time, I again "integrated" each of the test asteroids for 5000 yr and sampled the elements at every mapping period (48 yr). The results are histogrammed in Figs. 7 and 8. The histograms of Fig. 7 show the relative probabilities of the various semimajor axes and eccentricities using all the initial conditions of Fig. 5. This histogram of semimajor axes completely demolishes any remaining hopes that the statistical hypothesis is correct. There is only a faint hint of a dip in the distribution at the commensurability. Figure 8 shows the histograms for the initial conditions of Fig. 6. Even after time averaging there is a definite gap in the semimajor axes.

Although this is the first real demonstration of the formation of a gap, the gap is too narrow. The actual distribution of asteroid elements is shown in Fig. 9. The real Kirkwood gap is approximately twice as large. There seem to be two possible explanations for this discrepancy. Either the "integrations" were not continued for a long enough time (after all, two million years is still short compared to the age of the solar system) or some important physics has been left out. Two possibilities for the latter are the inclinations and the secular variations of Jupiter's orbit. In Sec. VI, I will extend the derivation of the mapping to include both the inclinations and the secular perturbations. That is, I will derive a mapping for the full resonance Hamiltonian (34).

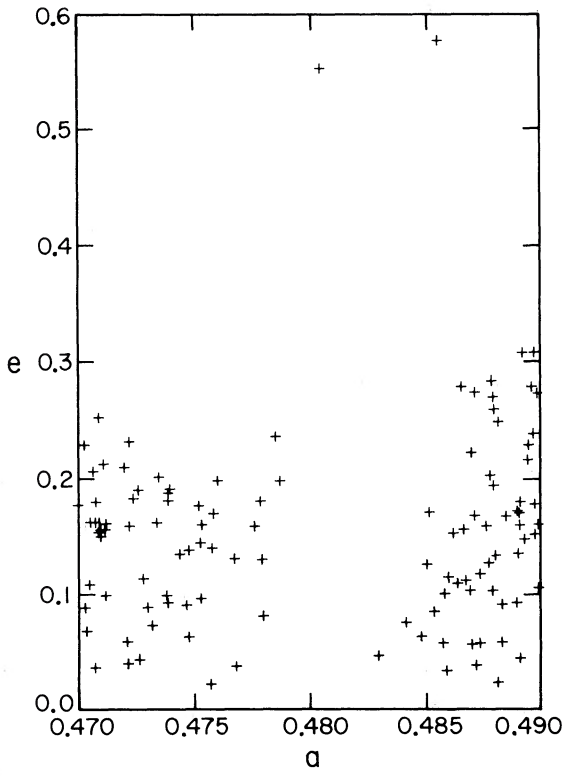

FIG. 9. The eccentricities vs semimajor axes for all asteroids in the TRIAD file with semimajor axes between 0.47 and 0.49.

VI. DERIVATION OF THE COMPLETE MAPPING

The mapping Hamiltonian for the complete resonant Hamiltonian, Eq. (34), is derived in exactly the same manner as was the planar-elliptic mapping Hamiltonian. It is

$$\begin{aligned} H_M = {} & \tfrac{1}{2}\alpha\Phi^2 + F_1(x_1^2 + y_1^2) + \bar{F}_1(x_1\xi_1 - y_1\eta_1) + F_2(x_2^2 + y_2^2) + \bar{F}_2(x_2\xi_2 - y_2\eta_2) \\ & - C_1(x_1^2 - y_1^2)2\pi\delta_{2\pi}[\Omega(t-\zeta_1)]\cos\varphi - D_1(x_1\xi_1 + y_1\eta_1)2\pi\delta_{2\pi}[\Omega(t-\zeta_2)]\cos\varphi \\ & - E_1(\xi_1^2 - \eta_1^2)2\pi\delta_{2\pi}[\Omega(t-\zeta_3)]\cos\varphi - C_2(x_2^2 - y_2^2)2\pi\delta_{2\pi}[\Omega(t-\zeta_4)]\cos\varphi \\ & - D_2(x_2\xi_2 + y_2\eta_2)2\pi\delta_{2\pi}[\Omega(t-\zeta_5)]\cos\varphi - E_2(\xi_2^2 - \eta_2^2)2\pi\delta_{2\pi}[\Omega(t-\zeta_6)]\cos\varphi \\ & - C_1 2x_1 y_1 2\pi\delta_{2\pi}[\Omega(t-\gamma_1)]\sin\varphi - D_1(x_1\eta_1 - y_1\xi_1)2\pi\delta_{2\pi}[\Omega(t-\gamma_2)]\sin\varphi \\ & + E_1 2\xi_1\eta_1 2\pi\delta_{2\pi}[\Omega(t-\gamma_3)]\sin\varphi - C_2 2x_2 y_2 2\pi\delta_{2\pi}[\Omega(t-\gamma_4)]\sin\varphi \\ & - D_2(x_2\eta_2 - y_2\xi_2)2\pi\delta_{2\pi}[\Omega(t-\gamma_5)]\sin\varphi + E_2 2\xi_2\eta_2 2\pi\delta_{2\pi}[\Omega(t-\gamma_6)]\sin\varphi. \end{aligned} \tag{107}$$

Again, the ζ_i and γ_i are arbitrary. I choose $0 \leqslant \zeta_1 < \zeta_2 < \zeta_3 < \zeta_4 < \zeta_5 < \zeta_6$ and $\pi/2\Omega \leqslant \gamma_1 < \gamma_2 < \gamma_3 < \gamma_4 < \gamma_5 < \gamma_6$, and let $\zeta_6 \to 0$ and $\gamma_6 \to \pi/2\Omega$. The secular motion between delta functions is

$$\begin{aligned} x_1(t) = {} & x_1(t_0)\cos[2F_1(t-t_0)] - y_1(t_0)\sin[2F_1(t-t_0)] \\ & - \bar{F}_1 \sum_k \frac{-d_k}{2F_1 - s_k}\{\cos(-s_k t + \delta_k) - \cos[-s_k t_0 + \delta_k - 2F_1(t-t_0)]\}, \end{aligned} \tag{108}$$

$$\begin{aligned} y_1(t) = {} & x_1(t_0)\sin[2F_1(t-t_0)] + y_1(t_0)\cos[2F_1(t-t_0)] \\ & + \bar{F}_1 \sum_k \frac{d_k}{2F_1 - s_k}\{\sin(-s_k t + \delta_k) - \sin[-s_k t_0 + \delta_k - 2F_1(t-t_0)]\}, \end{aligned} \tag{109}$$

$$\Phi(t) = \Phi(t_0), \tag{110}$$

$$\varphi(t) = \varphi(t_0) + (t-t_0)\alpha\Phi(t_0). \tag{111}$$

© American Astronomical Society • Provided by the NASA Astrophysics Data System

1982AJ.....87..577W

The solutions for $x_2(t)$ and $y_2(t)$ are similar to those for $x_1(t)$ and $y_1(t)$. The Hamiltonians during the first and fourth delta functions are of the form

$$H_{1,4} = -\frac{2\pi C_i}{\Delta\Omega}(x_i^2 - y_i^2)\cos\varphi, \tag{112}$$

where $i = 1$ for H_1 and $i = 2$ for H_4. This Hamiltonian is the same as the Hamiltonian during the first delta function of the planar-elliptic mapping. Thus the changes in the elements are

$$\Delta x_i = x_i\left[\cosh\left(\frac{4\pi C_i}{\Omega}\cos\varphi\right) - 1\right] - y_i \sinh\left(\frac{4\pi C_i}{\Omega}\cos\varphi\right), \tag{113}$$

$$\Delta y_i = y_i\left[\cosh\left(\frac{4\pi C_i}{\Omega}\cos\varphi\right) - 1\right] - x_i \sinh\left(\frac{4\pi C_i}{\Omega}\cos\varphi\right), \tag{114}$$

$$\Delta\Phi = -\frac{2\pi C_i}{\Omega}(x_i^2 - y_i^2)\sin\varphi, \tag{115}$$

and

$$\Delta\varphi = 0. \tag{116}$$

During the second and fifth delta functions the Hamiltonians have the form

$$H_{2,5} = -\frac{2\pi D_i}{\Delta\Omega}(x_i\xi_i + y_i\eta_i)\cos\varphi. \tag{117}$$

Again, $i = 1$ for H_2 and $i = 2$ for H_5. Consider just the $i = 1$ case, i.e., the second delta function. The equations of motion are

$$\dot{x}_1 = \frac{2\pi D_1}{\Delta\Omega}\eta_1\cos\varphi, \tag{118}$$

$$\dot{y}_1 = -\frac{2\pi D_1}{\Delta\Omega}\xi_1\cos\varphi, \tag{119}$$

$$\dot{\Phi} = -\frac{2\pi D_1}{\Delta\Omega}(x_1\xi_1 + y_1\eta_1)\sin\varphi, \tag{120}$$

and

$$\dot{\varphi} = 0. \tag{121}$$

Let t_0 be the time at which the delta function acts. Expanding ξ_1 and η_1 about $t = t_0$,

$$\xi_1(t_0 + \Delta t) = \xi_1(t_0) - \Delta t\sum c_k(-s_k)\times\sin(-s_k t_0 + \zeta_k) + o(\Delta t^2) \tag{122}$$

and

$$\eta_1(t_0 + \Delta t) = \eta_1(t_0) + \Delta t\sum c_k(-s_k)\times\cos(-s_k t_0 + \zeta_k) + o(\Delta t^2). \tag{123}$$

Substituting these into the equations of motion gives

$$\dot{x}_1 = \frac{2\pi D_1}{\Delta\Omega}\left(\eta_1(t_0) + \Delta t\sum c_k(-s_k)\times\cos(-s_k t_0 + \zeta_k) + o(\Delta t^2)\right) \tag{124}$$

and

$$\dot{y}_1 = \frac{2\pi D_1}{\Delta\Omega}\left(\xi_1(t_0) - \Delta t\sum c_k(-s_k)\times\sin(-s_k t_0 + \zeta_k) + o(\Delta t^2)\right). \tag{125}$$

These are trivially integrated to yield

$$x_1(t_0 + \Delta t) = x_1(t_0) + \Delta t\frac{2\pi D_1}{\Delta\Omega}\eta_1(t_0)\times\cos\varphi(t_0) + o\left(\frac{\Delta t^2}{\Delta}\right) \tag{126}$$

and

$$y_1(t_0 + \Delta t) = y_1(t_0) - \Delta t\frac{2\pi D_1}{\Delta\Omega}\xi_1(t_0)\times\cos\varphi(t_0) + o\left(\frac{\Delta t^2}{\Delta}\right). \tag{127}$$

Setting $\Delta t = \Delta$ and letting $\Delta\to 0$ gives the changes in x_1 and y_1:

$$\Delta x_1 = \frac{2\pi D_1}{\Omega}\eta_1\cos\varphi, \tag{128}$$

$$\Delta y_1 = -\frac{2\pi D_1}{\Omega}\xi_1\cos\varphi. \tag{129}$$

Substituting Eqs. (122), (123), (126), and (127) into the equation of motion for Φ gives

$$\dot{\Phi} = -\frac{2\pi D_1}{\Delta\Omega}\left(x_1(t_0)\xi_1(t_0) + y_1(t_0)\eta_1(t_0) - \Delta t\sum c_k(-s_k)[x_1(t_0)\sin(-s_k t_0 + \zeta_k) - y_1(t_0)\cos(-s_k t_0 + \zeta_k)] + o(\Delta t^2)\right)\sin\varphi(t_0). \tag{130}$$

Integrating, setting $\Delta t = \Delta$, and letting $\Delta\to 0$ yields

$$\Delta\Phi = -\frac{2\pi D_1}{\Omega}[x_1\xi_1 + y_1\eta_1]\sin\varphi. \tag{131}$$

Since the third and sixth delta functions do not involve x_i, y_i, or Φ, they can be integrated without a limiting procedure. The resulting changes in Φ are

$$\Delta\Phi = -\frac{2\pi E_i}{\Omega}(\xi_i^2 - \eta_i^2)\sin\varphi \tag{132}$$

for $i = 1$ and $i = 2$, respectively. The derivation of the changes across the other six delta functions are completely analogous. I give only the results. Across the seventh and tenth delta functions,

$$\Delta x_i = x_i\left[\exp\left(\frac{4\pi C_i}{\Omega}\sin\varphi\right) - 1\right], \tag{133}$$

$$\Delta y_i = y_i\left[\exp\left(-\frac{4\pi C_i}{\Omega}\sin\varphi\right) - 1\right], \tag{134}$$

© American Astronomical Society • Provided by the NASA Astrophysics Data System

1982AJ.....87..577W

and

$$\Delta\Phi = \frac{4\pi C_i}{\Delta\Omega} x_i y_i \cos\varphi. \tag{135}$$

The changes across the eighth and 11th delta functions are

$$\Delta x_i = -\frac{2\pi C_i}{\Omega}\xi_i \sin\varphi, \tag{136}$$

$$\Delta y_i = -\frac{2\pi C_i}{\Omega}\eta_i \sin\varphi, \tag{137}$$

and

$$\Delta\Phi = -\frac{2\pi D_i}{\Omega}(x_i\eta_i - y_i\xi_i)\cos\varphi. \tag{138}$$

Finally, across the ninth and 12th deltas,

$$\Delta\Phi = -\frac{4\pi E_i}{\Delta}\xi_i\eta_i \cos\varphi. \tag{139}$$

In Sec. VII, I display the results of some calculations using this mapping.

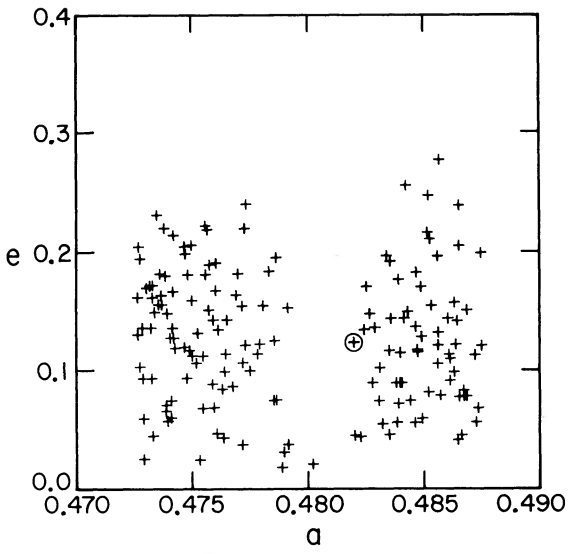

FIG. 10. Same as Fig. 6, but using the full mapping.

VII. FULL MAPPING CALCULATIONS

Using the full mapping ($\Omega = 1/4$), the same distribution of 300 test asteroids was "integrated" for two million years. The inclinations and nodes were taken from the TRIAD file as were the eccentricities before. So as not to prejudice the distribution with one particular set of the starting values for the phases of the secular terms [see Eqs. (30)–(33)], these phases were randomly chosen for each test asteroid. An asteroid is considered to be a Mars crosser if its eccentricity ever exceeds 0.3, thus the possibility of correlations among e, i, $\tilde{\omega}$, and Ω that prevent close encounters with Mars is ignored. The resulting distribution of asteroids that did not become Mars crossers is shown in Fig. 10. The time-averaged distributions are in Figs. 11 and 12. The gap is only slightly larger than before (cf. Figs. 6 and 8). The inclinations and secular terms do not seem to make much difference, at least in this two-million-year time interval. It remains a possibility that over much longer times more asteroids will show jumps in orbital eccentricity. The test asteroid that is circled in Fig. 8 was found to have a sudden increase in its eccentricity after 18 million years. This result is encouraging and indicates that indeed the full width of the gap might be reproduced if integrations of much longer time could be carried out.

VIII. SUMMARY AND CONCLUSIONS

The mappings in this paper are models for the motion of asteroids near the 3/1 commensurability. They have the correct secular and long-period resonant terms, but possess false high-frequency terms which are similar to high-frequency perturbations by Jupiter which have been neglected in previous work.

Mappings are useful for several reasons. First, they are a very fast (inexpensive) method for studying qualitatively what types of motion are possible near resonances. Second, within their approximations the mappings are more accurate since they are purely algebraic and hence use the full accuracy of the computer. "Integrations" using the mappings are thus valid for longer times than numerical integrations of the corresponding differential equations. Finally, and perhaps most importantly, the mappings include high-frequency contributions which are usually ignored yet seem to introduce new types of motion, i.e., the slow diffusion to a region of phase space where sudden large increases in eccentricity occur. The discovery of these sudden eccentricity increases introduced a new possibility for the origin of the Kirkwood gaps. The hypothesis is that asteroids near the commensurabilities undergo large jumps in eccentricity, thus becoming Mars crossers. They are subsequently removed from the gaps through collisions or close encounters with Mars. As a first test of this hypothesis I studied the evolution over two million years of a distribution of 300 test asteroids with initial conditions near the 3/1 commensurability. If Mars crossers are removed, a gap is produced at the proper location but it is too narrow, both in the planar-elliptic approximation and in the full three-dimensional problem with the secular perturbations of Jupiter's orbit included. There remains the possibility that two million years of evolution is too short. One orbit near the boundary of the gap in the mapping distribution was "integrated" for a much longer time and after 18 million years it had a sudden increase in its eccentricity. This implies that two million years is simply too short a time to see the full width of the gap to open. The difficulty is that even for the mapping 18 million years is a long time and it is not clear to

© American Astronomical Society • Provided by the NASA Astrophysics Data System

1982AJ.....87..577W

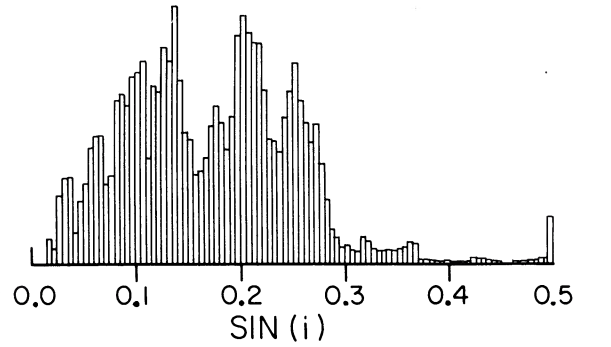

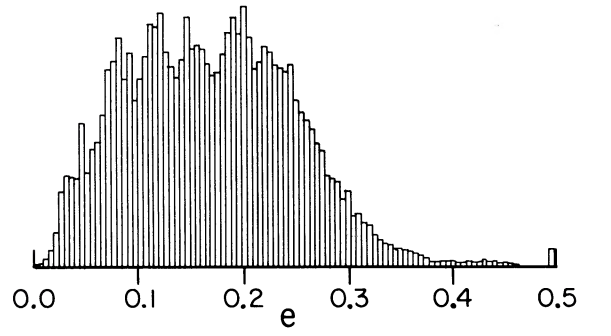

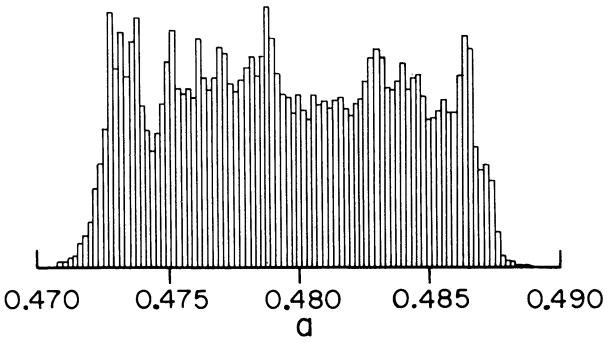

FIG. 11. Same as Fig. 7, but using the full mapping.

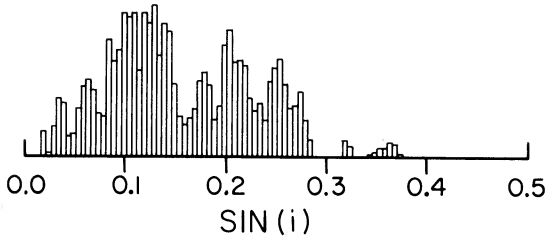

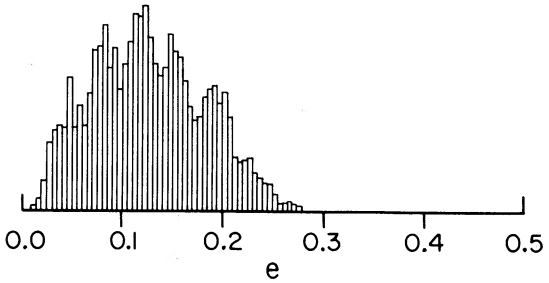

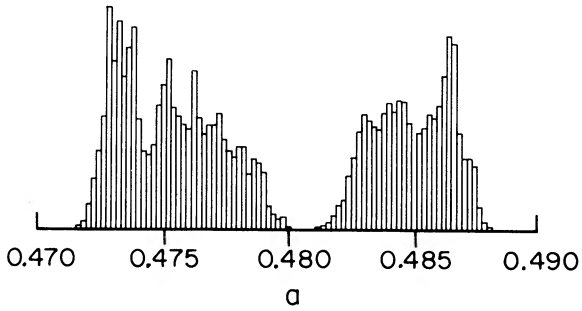

FIG. 12. Same as Fig. 8, but using the full mapping.

what extent the diffusion is due to the actual dynamics or to roundoff error.

A number of problems remain. The actual probability of collision with Mars must be estimated. This may be difficult since the behavior after the eccentricity increase is often very complicated. In some cases the eccentricity continues to increase in an erratic way, while in other cases, after a period of erratic behavior at large eccentricities, the eccentricity suddenly drops for a period of time to low values. Wetherill (1975) gives 200 million years as the typical lifetime for a Mars crosser. The lifetimes of the Mars crossers considered in this paper may be several times this value since they evidently spend only a fraction of their time with large enough eccentricity. To accurately estimate the collisional lifetimes may be a formidable task.

The other Kirkwood gaps are farther from Mars and asteroids will require higher eccentricities to be Mars crossers. It is still possible, though, that this mechanism will work since it was often the case, especially in the full three-dimensional mapping, that very large eccentricities (> 0.5) were obtained. Further consideration of the other Kirkwood gaps must await another study.

The mappings in this paper are only models for the motion of asteroids near the 3/1 commensurability. Those results which do not depend on the presence of the high-frequency perturbations are justified by the averaging principle. Thus the statistical hypothesis has been much more strongly disproved, and the removal of Mars crossers has been identified as a mechanism that is probably partially responsible for the origin of the 3/1 gap. The most novel and interesting result of this paper,

© American Astronomical Society • Provided by the NASA Astrophysics Data System

1982AJ.....87..577W

that test asteroids show sudden large increases in their eccentricity after sometimes millions of years, must be considered more speculative since it depends on the presence of the high-frequency terms. I have argued that in the first approximation it is the presence of the high-frequency terms that is important, not their exact form. Yet until this behavior is seen in an accurate numerical integration or until it is understood in an approximate analytic theory, this result cannot be fully believed.

It is a pleasure to thank Peter Goldreich for his encouragement and for the uncountably many discussions and suggestions without which this work would never have been done. It is also a pleasure to thank Hans Scholl and Claude Froeschlé for providing details of their calculations and for their continued interest. The data from the TRIAD file were generously provided by Jim Williams. This work was partially supported by NASA Grant No. NGL 05-002-003 and NSF Grant No. AST-8020005.

REFERENCES

Arnol'd, V. I. (1978). *Mathematical Methods of Classical Mechanics* (Springer, New York).
Arnol'd, V. I., and Avez, A. (1968). *Ergodic Problems of Classical Mechanics* (Benjamin, New York).
Brouwer, D., and Clemence, G. M. (1961). *Methods of Celestial Mechanics* (Academic, New York).
Brouwer, D., and van Woerkom, A. J. J. (1950). Astron. Pap. Am. Ephem. **13**, 81.
Chirikov, B. V. (1979). Phys. Rep. **52**, 263.
Froeschlé, C., and Scholl, H. (1976). Astron. Astrophys. **48**, 389.
Froeschlé, C., and Scholl, H. (1977). Astron. Astrophys. **57**, 33.
Giffen, R. (1973). Astron. Astrophys. **23**, 387.
Greenberg, R., and Scholl, H. (1979). *Asteroids* (University of Arizona, Tucson), p. 310.
Hénon, M., and Heiles, C. (1964). Astron. J. **69**, 73.
Heppenheimer, T. A. (1978). Astron. Astrophys. **70**, 457.
Ip, W.-H. (1979). Icarus **40**, 418.
Leverrier, U.-J. (1855). Ann. Obs. Paris, Mém. 1.
Moser, J. (1973). *Stable and Random Motions in Dynamical Systems* (Princeton University, Princeton, N.J.).
Moulton, F. R. (1970). *An Introduction to Celestial Mechanics* (Dover, New York).
Peirce, B. (1849). Astron. J. **1**, 1.
Plummer, H. C. (1960). *An Introductory Treatise on Dynamical Astronomy* (Dover, New York).
Poincaré, H. (1892). *Les Méthodes Nouvelles de la Mécanique Céleste* (Gauthier-Villars, Paris).
Scholl, H., and Froeschlé, C. (1974). Astron. Astrophys. **33**, 455.
Scholl, H., and Froeschlé, C. (1975). Astron. Astrophys. **42**, 457.
Schubart, J. (1964). Smithsonian Astrophys. Obs. Spec. Rep. No. 149.
Schubart, J. (1968). Astron. J. **73**, 99.
Schweizer, F. (1969). Astron. J. **74**, 779.
Wetherill, G. W. (1975). In *Proceedings of the Sixth Lunar Science Conference* (Pergamon, Oxford), p. 1539.
Wiesel, W. E. (1976). Celest. Mech. **13**, 3.
Wisdom, J. (1980). Astron. J. **85**, 1122.

© American Astronomical Society • Provided by the NASA Astrophysics Data System